A PATH FOLLOWING CONTROLLER FOR MODEL-SCALE HELICOPTERS

R. Cunha, C. Silvestre, A. Pascoal

Instituto Superior Técnico
Institute for Systems and Robotics
Torre Norte, piso 8, Av. Rovisco 1
1046-001 Lisboa, Portugal
e-mail:{rita,cjs,antonio}@isr.ist.utl.pt
fax:+351-218418291

Keywords: path following, gain scheduling control, unmanned air vehicles, guidance and control, dynamic modeling

Abstract

This paper addresses the problem of path following control system design for model-scale helicopters. The presented design strategy builds on the definition of an adequate generalized error space for expressing the vehicle's dynamics and kinematics. The path following problem is cast and solved in the framework of gain scheduling control theory, using the D-methodology. The resulting control law ensures that: i) the path following system achieves zero steady state tracking error about trimming trajectories, and ii) the linearizations of the nonlinear gain scheduled feedback system and the corresponding linear designs present the same internal as well as input-output characteristics. The controller performance is evaluated in simulation, using a helicopter nonlinear dynamic model parameterized for the Vario X-treme model-scale helicopter.

1 Introduction

Model-scale helicopters constitute one of the most versatile and cost-effective unmanned air vehicle (UAV) platforms currently used for the development and test of autonomous flight systems. The wide and valuable range of applications arising from the helicopter's maneuvering capabilities, allied to the increasing availability of accurate, reliable, and miniaturized sensors, justify the extensive research and development effort that is being undertaken worldwide. Unlike fixed-wing aircraft, helicopters were designed to describe vertical flight trajectories, including hovering and vertical take-off and landing (VTOL). Moreover, despite their ability to perform extremely agile maneuvers at high and low speeds, helicopters still provide good flying qualities in fast forward flight. The trade-off for this enhanced versatility is an inherent complexity that gives rise to a highly nonlinear and unstable dynamical system. In this context, the development of advanced guidance and control systems, based on accurate modeling of the helicopter's dynamics, is instrumental in bringing about high performance autonomous systems.

In this paper, the problem of steering a model-scale helicopter along predefined paths at a fixed speed is addressed. The solution follows the methodology described in [9], where the authors propose an integrated design of the guidance and control systems for autonomous vehicles, and present an implementation for the case of autonomous underwater vehicles. This methodology has two main advantages over traditional ones: i) stability of the combined guidance and control systems is guaranteed, and ii) the resulting path following system achieves zero steady state tracking error about trimming paths.

The design method builds on three key results: i) the trimming trajectories associated to trimming paths of helicopters are helices parameterized by the vehicle's linear speed, yaw rate, and flight path angle (trimming vector); ii) steering the vehicle along a trimming path at constant speed is equivalent to driving a generalized tracking error to zero, and iii) the linearization of the generalized error dynamics about any trimming path is time-invariant. In view of these results, the problem of steering a vehicle along a piecewise continuous concatenation of trimming paths can be tackled using gain scheduling [8]. The adopted methodology uses the D-methodology described in [5], implementing a gain scheduled controller, which ensures the equivalence between the linearization of the nonlinear closed-loop system and the corresponding linear designs.

The paper is organized as follows. Section 2 describes a general dynamic model for a model-scale helicopter. Section 3 introduces the concepts of trimming trajectories and paths and defines a generalized error space for describing the vehicle's motion. Section 4 describes the methodology for the design of a gain scheduled path following controller and outlines its implementation. Section 5 presents simulation results for the path following controller obtained with the helicopter nonlinear dynamic simulator *SimModHeli*. Section 6 concludes the paper highlighting the main features of the proposed control system.

2 Helicopter dynamic model

The helicopter dynamic model presented hereafter was the basis for the development of a simulator, named *SimModHeli* [2], implemented in Matlab, using Simulink and C MEX-file S-functions, that will be made freely available for the scientific community. This simulator is completely parameterizable and describes the dynamics of helicopters with any number of

blades, with or without a Hiller or Bell-Hiller stabilizing bar. The simulation model is specially tailored for model-scale helicopters, such as the one depicted in Figure 1, and includes the rigid body, main rotor flapping, and stabilizing bar dynamics. The dynamics of the helicopter can be described using a six

Figure 1: Vario X-Treme helicopter

degree of freedom rigid body model driven by forces and moments that explicitly include the effects of the main rotor, Bell-Hiller stabilizing bar, tail rotor, fuselage, horizontal tailplane, and vertical fin. To derive the equations of motion, the following notation is required:

$\{U\}$ - universal coordinate frame;
$\{B\}$ - body-fixed coordinate frame, with origin at the vehicle's centre of mass;
$\mathbf{p} = \left[\, x \;\; y \;\; z \,\right]^T$ - position of the vehicle's center of mass, expressed in $\{U\}$;
$\boldsymbol{\lambda} = \left[\, \phi \;\; \theta \;\; \psi \,\right]^T$ - *Z-Y-X* Euler angles that parameterize locally the orientation of the vehicle relative to $\{U\}$;
$\mathbf{v} = \left[\, u \;\; v \;\; w \,\right]^T$ - body-fixed linear velocity vector;
$\boldsymbol{\omega} = \left[\, p \;\; q \;\; r \,\right]^T$ - body-fixed angular velocity vector.

Figure 2 captures the general structure of the helicopter model that can be written as

$$\begin{cases} \dot{\mathbf{v}} = F_v\left(\mathbf{v}, \boldsymbol{\omega}, \boldsymbol{\lambda}, \mathbf{u}\right) \\ \dot{\boldsymbol{\omega}} = F_\omega\left(\mathbf{v}, \boldsymbol{\omega}, \boldsymbol{\lambda}, \mathbf{u}\right) \\ \dot{\mathbf{p}} = R\left(\boldsymbol{\lambda}\right)\mathbf{v} \\ \dot{\boldsymbol{\lambda}} = Q\left(\boldsymbol{\lambda}\right)\boldsymbol{\omega} \end{cases}, \tag{1}$$

with

$$F_v\left(\mathbf{v}, \boldsymbol{\omega}, \boldsymbol{\lambda}\right) = -\boldsymbol{\omega} \times \mathbf{v} + \mathbf{f}\left(\boldsymbol{\lambda}\right)/m, \tag{2}$$

$$F_\omega\left(\mathbf{v}, \boldsymbol{\omega}, \boldsymbol{\lambda}\right) = -I^{-1}\left[\, \boldsymbol{\omega} \times I\boldsymbol{\omega} + \mathbf{n}\left(\mathbf{v}, \boldsymbol{\omega}, \mathbf{u}\right)\right], \tag{3}$$

where m is the vehicle's mass, I is the tensor of inertia about the $\{B\}$ frame, $\mathbf{f}$ and $\mathbf{n}$ are the vectors of external forces and moments respectively along the same frame, $\mathbf{f}_g$ is the gravitational force also expressed in $\{B\}$, R is the rotation matrix from $\{B\}$ to $\{U\}$, and Q is the transformation from angular speeds to Euler angle derivatives. The external force and moment vectors are functions of the vehicle velocities and of the command vector $\mathbf{u} = \left[\, \delta_0 \;\; \delta_{1c} \;\; \delta_{1s} \;\; \delta_{0t} \,\right]^T$ that consists of the main rotor collective input δ_0, main rotor and flybar cyclic inputs δ_{1c} and δ_{1s}, and tail rotor collective input δ_{0t}.

The following sections present mathematical models for the main rotor and Bell-Hiller stabilizing bar. A comprehensive

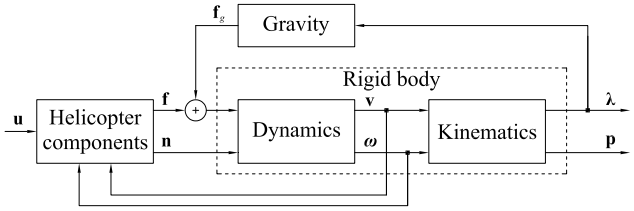

Figure 2: Helicopter model - block diagram

study of helicopter dynamic modeling, including the remaining helicopters components can be found in [3]. For in-depth coverage of helicopter flight dynamics, the reader is referred to [4, 6, 7].

2.1 Main rotor

In rotary-wing aircraft, the main rotor is not only the dominant system, but also the most complex one. It is the primary source of lift, which counteracts the body weight and sustains the helicopter in air. Additionally, the main rotor generates other forces and moments that enable the control of the aircraft position, orientation and velocity. This section presents a simplified rotor dynamic model, whose main building blocks are depicted in Figure 3.

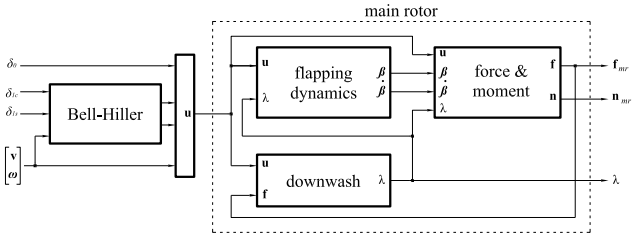

Figure 3: Main rotor block diagram

The model adopted to describe the rotor blades is standard and assumes that these are rigid and linked to the hub through flap hinge springs, with stiffness k_β [6]. The dynamic behaviour is thus confined to the flapping motion that can be described by vector $\boldsymbol{\beta} = \left[\, \beta_0 \;\; \beta_{1c} \;\; \beta_{1s} \,\right]^T$, where β_0 denotes the collective mode (also called coning), and β_{1c} and β_{1s} the longitudinal and lateral cyclic modes, respectively. This vector corresponds to the constant and first-order harmonics of the Fourier Series expansion of the flapping angle β, expressed as function of the blade azimuth angle $\psi = \Omega t$ (Ω denotes the rotor angular speed). The equations of motion for a flapping rotor, expressed in the main rotor wind-aligned frame, can be approximated by the following second-order system

$$\begin{aligned} \ddot{\boldsymbol{\beta}} + \Omega A_{\dot{\boldsymbol{\beta}}}(\mu)\dot{\boldsymbol{\beta}} + \Omega^2 A_{\boldsymbol{\beta}}(\mu)\boldsymbol{\beta} = \Omega^2 B_\theta(\mu)\begin{bmatrix} \theta_0 \\ \theta_{1c} \\ \theta_{1s} \end{bmatrix} + \\ \Omega^2 B_\omega(\mu)\begin{bmatrix} \bar{p} \\ \bar{q} \end{bmatrix} + \Omega^2 B_\lambda(\mu)\begin{bmatrix} \mu_z - \lambda_0 \\ \lambda_{1c} \\ \lambda_{1s} \end{bmatrix}, \end{aligned} \tag{4}$$

where, according to standard notation in helicopter theory [6],

the helicopter velocities are normalized, with μ and μ_z denoting the forward and vertical velocities, respectively, and $\bar{p}$ and $\bar{q}$ the roll and pitch rates, respectively. The induced downwash is also normalized and decomposed into constant λ_0 and sinusoidal components λ_{1c} and λ_{1s}. It should be noted that, for control system design purposes, the flapping motion as described by (4) preserves a high degree of accuracy, while rendering a much more tractable system. For instance, the coefficient matrices in (4) depend solely on the helicopter forward velocity.

Control of the blade aerodynamic loads, which ultimately determines the main rotor force and moment contributions ($\mathbf{f}_{mr}$ and $\mathbf{n}_{mr}$), is obtained by changing the blade pitch angle θ as function of the rotor command inputs. Without the Bell-Hiller system and neglecting the servo actuator dynamics, the blade pitch angle is given by

$$\theta(\psi) = \delta_0 + \delta_{1c}\cos(\psi) + \delta_{1s}\sin(\psi). \tag{5}$$

In systems equipped with the Bell-Hiller stabilizing bar, only the collective input δ_0 is directly applied to the main rotor. The cyclic inputs δ_{1c} and δ_{1s} are mixed with the motion of the bar to determine the actual cyclic components (θ_{1c} and θ_{1s}) applied to blade pitch links. The equations of motion for these components are presented in the next section.

Using either the dynamic or the steady-state solution for the flapping equation (4), the main rotor forces and moments at the hub can be written as

$$\mathbf{f}_{mr} = \frac{n}{2}\begin{bmatrix} -Y_{1s} \\ -Y_{1c} \\ 2Z_0 \end{bmatrix} + \frac{n}{2}\begin{bmatrix} -Z_{1c} & -Z_0 & 0 \\ Z_{1s} & 0 & Z_0 \\ 0 & 0 & 0 \end{bmatrix}\begin{bmatrix} \beta_0 \\ \beta_{1c} \\ \beta_{1s} \end{bmatrix}, \tag{6}$$

and

$$\mathbf{n}_{mr} = n\begin{bmatrix} 0 \\ 0 \\ N_0 \end{bmatrix} + \frac{n}{2}\begin{bmatrix} -N_{1c} & -N_0 & -k_\beta \\ N_{1s} & -k_\beta & N_0 \\ 0 & 0 & 0 \end{bmatrix}\begin{bmatrix} \beta_0 \\ \beta_{1c} \\ \beta_{1s} \end{bmatrix}. \tag{7}$$

The $Y_{(.)}$, $Z_{(.)}$, and $N_{(.)}$ terms, in (6) and (7), represent the force and moment components generated by the blades. These quantities are functions of the helicopter state variables and main rotor inputs. Explicit expressions and a detailed description of these terms can be found in [3].

2.2 Bell-Hiller stabilizing bar

The Bell-Hiller stabilizing bar, a mechanical blade pitch control system that improves helicopter stability, is currently a standard component in model-scale helicopters. From a control point of view, the stabilizing bar can be interpreted as a dynamic feedback system for the roll and pitch rates. The system consists of a so-called flybar (a teetering rotor placed at a 90^o rotation interval from the main rotor blades and tipped on both ends by aerodynamic paddles) and a mixing device that combines the flybar flapping motion with the cyclic inputs to determine the cyclic pitch angle applied to the main rotor blades. The flybar and main rotor flapping motions are governed by the same effects, namely the gyroscopic moments due the helicopter roll and pitch rates. However, unlike the main rotor, the flybar is not responsible for providing lift or maneuvering ability. Thus, it can be designed to have a slower response and provide the desired stabilization effect.

The notation used to describe the Bell-Hiller system is presented in Figure 4, where the mechanical arrangement for the X-Treme helicopter is reproduced.

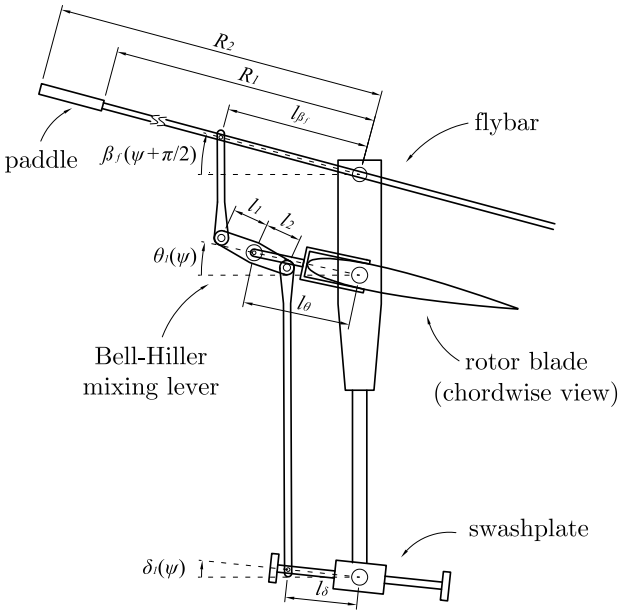

Figure 4: Bell-Hiller system with angular displacements

Due to the geometric constraint introduced by the mixing lever, the flybar flapping and rotor blade pitching motions are effectively combined. The equations of motion for the main rotor blade pitching can be written as

$$\begin{bmatrix} \ddot{\theta}_{1c} \\ \ddot{\theta}_{1s} \end{bmatrix} + \Omega A_{\dot{\theta}}\begin{bmatrix} \dot{\theta}_{1c} \\ \dot{\theta}_{1s} \end{bmatrix} + \Omega^2 A_\theta(\mu)\begin{bmatrix} \theta_{1c} \\ \theta_{1s} \end{bmatrix} = \Omega^2 B_\delta(\mu)\begin{bmatrix} \delta_{1c} \\ \delta_{1s} \end{bmatrix} + \Omega^2 B_\omega\begin{bmatrix} \bar{p} \\ \bar{q} \end{bmatrix} + \Omega^2 B_\lambda(\mu)\begin{bmatrix} \mu_z - \lambda_0 \\ \lambda_{1c} \\ \lambda_{1s} \end{bmatrix}. \tag{8}$$

The blade pitching motion, in particular its response to helicopter shaft rotations, depends on the physical parameters of the Bell-Hiller system, namely the lever arms l_1, and l_2, the flybar radii R_1 and R_2, and the flybar Lock number defined as

$$\gamma_f = \rho c_f a_{0_f}\left(R_2^4 - R_1^4\right)/I_{\beta_f}, \tag{9}$$

where ρ is the air density, c_f the paddle chord, a_{0_f} the paddle lift curve slope, and I_{β_f} the flybar moment of inertia. Therefore, there are several different means of adjusting the flybar stabilizing effect. Changing the shape, weight or distance between the paddles or the ratio between the mixing lever arms l_1 and l_2 are all straightforward ways of achieving this variation (see [1] for further details).

3 Generalized error dynamics

This section introduces the concepts of trimming trajectories and paths for the helicopter model, presents a generalized error space to describe the helicopter's motion about trimming paths, and computes explicitly the helicopter dynamics in the new error space.

Consider the helicopter equations of motion presented in (1), and let $\mathbf{v}_c$, $\boldsymbol{\omega}_c$, $\mathbf{p}_c$, $\boldsymbol{\lambda}_c$, and $\mathbf{u}_c$ denote the trimming values of the state and input vectors. At trimming, these vectors satisfy

$$\begin{cases} \dot{\mathbf{v}}_c = F_v\left(\mathbf{v}_c, \boldsymbol{\omega}_c, \boldsymbol{\lambda}_c, \mathbf{u}_c\right) = \mathbf{0} \\ \dot{\boldsymbol{\omega}}_c = F_\omega\left(\mathbf{v}_c, \boldsymbol{\omega}_c, \boldsymbol{\lambda}_c, \mathbf{u}_c\right) = \mathbf{0} \end{cases}, \tag{10}$$

implying that $\dot{\mathbf{u}}_c = \mathbf{0}$, $\dot{\phi}_c = 0$, and $\dot{\theta}_c = 0$. Given the dependence of the gravitational terms on the roll and pitch angles, only the yaw angle can change without violating the equilibrium condition. However, ψ_c satisfies

$$\begin{bmatrix} 0 \\ 0 \\ \dot{\psi}_c \end{bmatrix} = Q\left(\boldsymbol{\lambda}_c\right)\boldsymbol{\omega}_c, \tag{11}$$

and thus the yaw rate, $\dot{\psi}_c$, is constant. As shown in [9], trimming trajectories correspond to helices that can be described by

$$\dot{\boldsymbol{\lambda}}_c = \begin{bmatrix} 0 \\ 0 \\ \dot{\psi}_c \end{bmatrix}, \dot{\mathbf{p}}_c = \begin{bmatrix} V_c\cos(\gamma_c)\cos(\dot{\psi}_c t + \psi_0) \\ V_c\cos(\gamma_c)\sin(\dot{\psi}_c t + \psi_0) \\ -V_c\sin(\gamma_c) \end{bmatrix}, \tag{12}$$

where $V_c = \|\mathbf{v}_c\|$ is the linear body speed, γ_c the flight-path angle, and ψ_0 the helix initial condition. The helix can thus be described by the following parameterization

$$\eta_c = \begin{bmatrix} V_c & \gamma_c & \dot{\psi}_c & \psi_0 \end{bmatrix}^T. \tag{13}$$

The time-independent 3D curve described by a vehicle that is tracking a trimming trajectory is usually called a trimming path, and is here denoted by Γ_c.

The definition of the error vector requires the introduction of the following additional notation, which relates the vehicle's current state with the desired state on the trimming path.

$\mathbf{d}$ - Distance vector from the vehicle's current position $\mathbf{p}$ to the closest point $\mathbf{p}_c$ on the path, expressed in $\{U\}$.

$\{T\}$ - Tangent frame, whose x, y and z axes correspond to the tangent, normal, and binormal to the curve at $\mathbf{p}_c$. Note that the distance vector expressed in $\{T\}$ takes the form $\mathbf{d}_T = [0, y_d, z_d]$.

$\{C\}$ - Command frame, defined as coincident with the body frame $\{B\}$ when the vehicle follows the trimming path. Notice that $\{C\}$ is not necessarily aligned with $\{T\}$.

The graphical representation of these frames and vectors is presented in Figure 5. Let the generalized error vector be given by

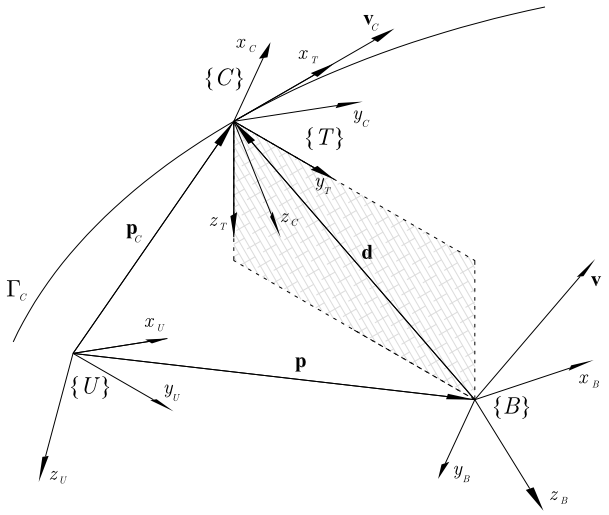

Figure 5: Path following notation

$$\begin{cases} \mathbf{v}_e = \mathbf{v} - \mathbf{v}_c \\ \boldsymbol{\omega}_e = \boldsymbol{\omega} - \boldsymbol{\omega}_c \\ \mathbf{d}_\pi = \Pi R^{-1}\mathbf{d} \\ \boldsymbol{\lambda}_e = Q^{-1}(\boldsymbol{\lambda} - \boldsymbol{\lambda}_c) \end{cases}, \tag{14}$$

where Π is the projection matrix

$$\Pi = \begin{bmatrix} 0 & 1 & 0 \\ 0 & 0 & 1 \end{bmatrix} \tag{15}$$

that selects the last two components of a vector. It should be noted that $\mathbf{d}$ is defined as the distance to the trimming path and not to the trimming trajectory. It is easily shown that the vehicle is following a path Γ_c at a constant speed V_c if and only if the generalized error vector defined in (14) is zero [9]. This equivalence breaks down when the trimming velocity has no forward component relative to the trimming path, i.e., when $\mathbf{v}_{c_T} = [0, v_y, v_z]^T$. The type of trimming paths tackled in this paper do not violate the referred validity condition. The rigid body equations of motion, expressed in the new error space can be written as

$$\begin{cases} \dot{\mathbf{v}}_e = \dot{\mathbf{v}} \\ \dot{\boldsymbol{\omega}}_e = \dot{\boldsymbol{\omega}} \\ \dot{\mathbf{d}}_\pi = F_{\mathbf{d}_\pi}(\mathbf{v}_e, \boldsymbol{\omega}_e, \mathbf{d}_\pi, \boldsymbol{\lambda}_e) \\ \dot{\boldsymbol{\lambda}}_e = F_{\boldsymbol{\lambda}_e}(\mathbf{v}_e, \boldsymbol{\omega}_e, \boldsymbol{\lambda}_e) \end{cases}, \tag{16}$$

where $\mathbf{u}_e = \mathbf{u} - \mathbf{u}_c$, and $F_{\mathbf{d}_\pi}$ and $F_{\boldsymbol{\lambda}_e}$ are obtained from (1) and (14).

The following fundamental result arises from the definition of the error space: the linearization of (16) about the zero solution, or equivalently, the linearization of the rigid body dynamics about the trimming path, expressed in the generalized error space, is time-invariant (see [9] for full details). The linearized system can be written as

$$\begin{cases} \delta\dot{\mathbf{v}}_e = A_v^v\delta\mathbf{v}_e + A_v^\omega\delta\boldsymbol{\omega}_e + A_v^\lambda\delta\boldsymbol{\lambda}_e + B_v\delta\mathbf{u}_e \\ \delta\dot{\boldsymbol{\omega}}_e = A_\omega^v\delta\mathbf{v}_e + A_\omega^\omega\delta\boldsymbol{\omega}_e + A_\omega^\lambda\delta\boldsymbol{\lambda}_e + B_\omega\delta\mathbf{u}_e \\ \delta\dot{\mathbf{d}}_\pi = L_c({}^C_T R, \boldsymbol{\omega}_c)\,\delta\mathbf{d}_\pi + J_c({}^C_T R)\left[-\mathbf{v}_c \times \delta\boldsymbol{\lambda}_e + \delta\mathbf{v}_e\right] \\ \delta\dot{\boldsymbol{\lambda}}_e = \delta\boldsymbol{\omega}_e - \boldsymbol{\omega}_c \times \delta\boldsymbol{\lambda}_e \end{cases}, \tag{17}$$

where the coefficient matrices for the dynamics are computed at trimming according to

$$A_x^y = \frac{\partial}{\partial \mathbf{y}} \left[F_x(.)\right]\Big|_c \text{ and} B_x = \frac{\partial}{\partial \mathbf{u}} \left[F_x(.)\right]\Big|_c \qquad (18)$$

and the coefficients for the kinematics are functions of ${}^C_T R$ the constant rotation matrix from $\{T\}$ to $\{C\}$, and $\mathbf{v}_c$ and $\boldsymbol{\omega}_c$ the command velocities.

From this result, it follows that associated with each trimming path $\Gamma(\eta_c)$ there is a linear time-invariant plant (17) for which a linear controller can be designed.

4 Control system design and implementation

Following the methodology described in [5, 9], the result stated in the previous section can be used to design a path following controller based on gain scheduling. The controller design procedure can be described as follows:

- Select a finite set of trimming paths parameterized by η_c.
- Linearize the corresponding generalized error plants about the selected trimming paths.
- Design linear controllers with integral action on selected states to achieve adequate performance for each of the linear plants.
- Implement a non-linear gain scheduled controller, using the D-methodology [5].

The structure of the linear systems given in (17), can be rewritten in the more condensed form as

$$\delta\dot{\mathbf{x}}_e = A(\eta_c)\delta\mathbf{x}_e + B(\eta_c)\delta\mathbf{u}_e, \qquad (19)$$

where

$$\delta\mathbf{x}_e = [\delta\mathbf{v}_e^T, \delta\boldsymbol{\omega}_e^T, \delta\mathbf{d}_\pi^T, \delta\boldsymbol{\lambda}_e^T]^T ,$$

and the coefficients for the dynamics in $A(\eta_c)$ and $B(\eta_c)$ are obtained from the linearization of the full nonlinear model about the trimming path parameterized by η_c.

In the design of the linear controllers, integrators are appended to selected state variables to ensure zero steady state errors. The structure of the linear controllers, which are synthesized using the state feedback LQR synthesis technique, is given by

$$\begin{cases} \delta\dot{\mathbf{x}}_c = L_x\delta\mathbf{x}_e \\ \delta\mathbf{u}_e = K_{l_1}(\eta_c)\delta\mathbf{x}_e + K_{l_2}(\eta_c)\delta\mathbf{x}_c \end{cases}, \qquad (20)$$

where matrix L_x selects the variables to be integrated.

Given the set of linear controllers, the D-methodology can be applied. This design method amounts to moving all integrators to the plant input, adding derivators where needed to preserve the transfer functions. Assuming that K_{l_2} is square ($\dim(\mathbf{x}_c) = \dim(\mathbf{u})$) and invertible, the following *linearization property* is satisfied: the linearizations of the nonlinear closed-loop system about trimming paths preserve the same internal as well as input-output properties of the corresponding linear closed loop designs [9].

In the current implementation, $\dot{\mathbf{x}}_c$ comprises u_e, v_e, and $\mathbf{d}_\pi$, ensuring exact tracking of the trimming path. The resulting nonlinear gain scheduled controller, depicted in Figure 6, is given by

$$\begin{cases} u_e = u - u_c \\ v_e = v - v_c \\ \mathbf{d}_\pi = \Pi R^{-1}(\mathbf{p}_c - \mathbf{p}) \\ \dot{\mathbf{x}}_c = K_1(\eta)[\dot{\mathbf{v}}^T \dot{\boldsymbol{\omega}}^T \dot{\mathbf{d}}_\pi^T \dot{\boldsymbol{\lambda}}_e^T]^T + K_2(\eta)[u_e\, v_e\, \mathbf{d}_\pi^T]^T \\ \mathbf{u} = \mathbf{x}_c \end{cases}, \qquad (21)$$

with $\boldsymbol{\omega} - Q^{-1}\dot{\boldsymbol{\lambda}}_c$ replacing $\dot{\boldsymbol{\lambda}}_e$, since both yield the same expression when linearized about the trimming path. In Figure 6, block E is responsible for the computation of the error state variables u_e, v_e, and $\mathbf{d}_\pi$, given the original state variables $\mathbf{v}$, $\mathbf{p}$, and $\boldsymbol{\lambda}$, the desired path Γ_c, and the forward velocity V_c. The gain matrix $K(\eta)$ is selected according to the scheduling variable $\eta = [V, \gamma, \psi]$.

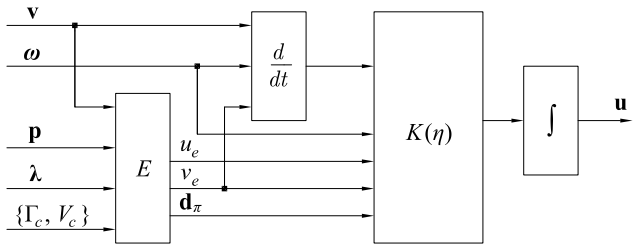

Figure 6: Nonlinear path following controller

In addition to solving the path following problem for all trimming paths and alongside the already stated linearization property, the nonlinear control implementation has other important properties, which are worthwhile emphasizing: i) *auto-trimming property* - the controller automatically generates adequate trimming values for the actuation signals and for the state variables that are not required to track reference inputs; ii) the implementation of anti-windup schemes is straightforward, due to the placement of the integrators at the plant input.

5 Simulation results

This section presents the simulation results obtained with the described path following controller. The closed loop system was implemented using the helicopter nonlinear dynamic model simulator *SimModHeli*[2], parameterized for the Vario X-Treme model-scale helicopter. The path to be followed was defined about the reference speed of 2 m/s, and consists of: i) keeping the helicopter in level flight along the x axis, ii) tracking a climbing helix, and iii) tracking a positive ramp in the yoz plane, see Figure 7. The parameters and initial position of each of these stages are presented in Table 1. The controller was tested introducing a perturbation on the initial position of the helicopter, which was set to $\mathbf{p}_0 = [0\ -4\ -2]^T$ m. All other state variables were set to the previously computed trimming values. The path described by the helicopter and corresponding actuation signals are illustrated in Figures 7 and 8, respectively.

	V_c (m/s)	γ_c (deg)	$\dot{\psi}_c$ (deg/s)	ψ_0 (deg)	$\mathbf{p}_0$(m)
i)	2	0	0	0	$[\ 0\ \ 0\ \ 0\ ]^T$
ii)	2	19.5	13.5	0	$[20\ \ 0\ \ 0\ ]^T$
iii)	2	10	0	270	$[12\ \ 8\ \ 13.4]^T$

Table 1: Parameters for the reference path

At the beginning of the maneuver, the helicopter quickly converges to the desired path through a combination roll and yaw angular motions, mainly commanded by the longitudinal cyclic δ_{1c} and tail rotor collective δ_{0t}. The aircraft continues on track through the remainder of the maneuver, with only slight deviations during the transition between stages.

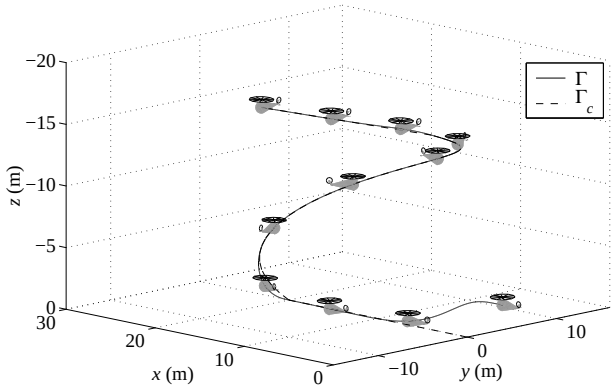

Figure 7: Path following simulation, 3D view

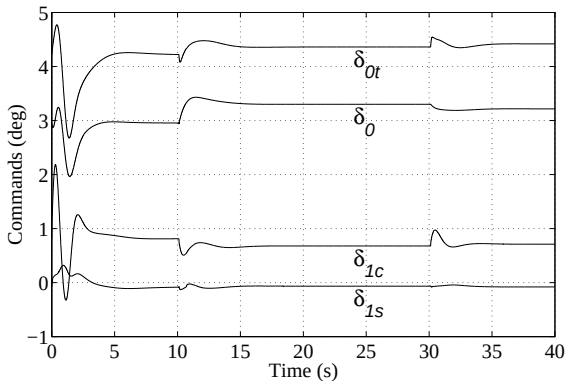

Figure 8: Blade pitch angle commands

6 Concluding remarks

The paper presented a new methodology for the design of path following controllers for helicopters. The design method builds on three key results: i) the trimming trajectories associated to trimming paths of helicopters are helices parameterized by the vehicle's linear speed, yaw rate, and flight path angle (trimming vector); ii) steering the vehicle along a trimming path at constant speed is equivalent to driving a generalized tracking error to zero, and iii) the linearization of the generalized error dynamics about any trimming path is time-invariant. Based on these results, the problem of path following system design was cast and solved in the framework of gain scheduling control theory.

A key feature of the controllers developed is their ability to automatically generate the trimming values for the plant inputs and for all state variables that are not required to track reference inputs. This is in sharp contrast to traditional designs where feedforwarding of these values is required. The new methodology is simple to apply and leads to a nonlinear controller with a structure similar to that of the original linear designs. The performance of the controllers was assessed in simulation.

Acknowledgements

This work was (partially) supported by the FCT Programa Operacional Sociedade de Informação (POSI) in the frame of QCA III and by the POSI/SRI/41938/2001 ALTICOPTER project. The work of R. Cunha was supported by a PhD Student Scholarship from the POCTI Programme of FCT, SFRH/BD/5034/2001.

References

[1] R. Cunha, C. Silvestre, "Dynamic Modeling and Stability Analysis of Model-Scale Helicopters With Bell-Hiller Stabilizing Bar", *AIAA Guidance, Navigation, and Control Conference*, Austin, TX, USA, (2003).

[2] R. Cunha, C. Silvestre, "SimModHeli: A Dynamic Simulator for Model-Scale Helicopters", *11th Mediterranean Conference on Control and Automation MED'03*, Rhodes, Greece, (2003).

[3] R. Cunha. "Modeling and control of an autonomous robotic helicopter", MSc thesis, Department of Electrical and Computer Engineering, Instituto Superior Técnico, Portugal, (2002), in english.

[4] W. Johnson. *Helicopter Theory*, Dover Publications, New York, USA, (1994).

[5] I. Kaminer, A. Pascoal, E. Hallberg, C.Silvestre. "Trajectory Tracking for Autonomous Vehicles: An Integrated Approach to Guidance and Control", *AIAA Journal of Guidance, Control, and Dynamics*, **21(1)**, pp. 29–38, (1998).

[6] G. D. Padfield. *Helicopter Flight Dynamics: The Theory and Application of Flying Qualities and Simulation Modeling*, AIAA Education Series, Washington, USA, (1996).

[7] R. W. Prouty. *Helicopter Performance, Stability, and Control*, Krieger Publishing Company, Florida, USA, (1995).

[8] W. J. Rugh, J. S. Shamma. "A Survey of Research on Gain Scheduling", *Automatica*, **36(9)**, pp. 1401–1425, (2000).

[9] C. Silvestre, A. Pascoal, I. Kaminer. "On the Design of Gain-Scheduled Trajectory Tracking Controllers", *International Journal of Robust and Nonlinear Control*, **12**, pp. 797-839, (2002).